

IZOD impact properties of full-density fused deposition modeling polymer materials with respect to raster angle and print orientation

Albert E Patterson^{1,2} , Tais Rocha Pereira^{2,3}, James T Allison¹ and Sherri L Messimer²

Proc IMechE Part C:
J Mechanical Engineering Science
2021, Vol. 235(10) 1891–1908
© IMechE 2019
Article reuse guidelines:
sagepub.com/journals-permissions
DOI: 10.1177/0954406219840385
journals.sagepub.com/home/pic



Abstract

One of the fundamental characteristics of additively processed materials is that they are naturally anisotropic; this variance in mechanical properties is primarily generated through the formulation of patterned *shell* and *in-filled* regions within the material during processing. This paper describes the formulation and results of a study to ascertain the impact strength of various full-infill polymer-based materials processed in various orientations and angles via fused deposition modeling. Ten different materials were tested using seven different hatch angles and three print orientations. Seven different pure materials were tested, as well as three composites; these were acrylonitrile butadiene styrene, standard polylactic acid, high-temperature polylactic acid, high-impact polystyrene, nylon, polyethylene terephthalate + glycol, polycarbonate, aluminum polylactic acid, wood polylactic acid, and carbon-fiber polylactic acid. All experiments were carried out using ASTM IZOD Type E tests with a 2.7J pendulum. Five replications of each test combination were collected, for a total of 1050 tests. The results showed that the shell orientation and raster angle were primary drivers in determining impact properties, as they strongly influenced the crack length and path through the material during fracture. This was especially clear for the polycarbonate, nylon, and polyethylene terephthalate + glycol which underwent large plastic deformation during the tests. It was further observed that the impact toughness was inversely correlated with test repeatability, with the toughest materials having the highest variability between test replications.

Keywords

Fused deposition modeling, IZOD testing, 3-D printing, material mesostructure, materials testing

Date received: 24 September 2018; accepted: 6 March 2019

Introduction

The rise and rapid maturity of additive manufacturing (AM) processes in recent decades have brought much benefit to engineering design, opening up an entire new series of possible manufacturing processes. The fundamental characteristic (and most beneficial aspect) of AM processes is the ability to directly manufacture products in layers from CAD models without the need for dedicated tooling. There are a large number of processes, roughly divided into seven families^{1,2} based on the state of the raw material, the layering technique, and the layer fusion method.

Despite the great design freedom gained from the use of AM, however, a serious consideration of the materials thus produced is their strong natural anisotropy.^{3–6} Due to this variance throughout the bulk, AM materials have a strongly defined mesostructure, in addition to the typical micro- and

macrostructure.^{7–9} This could be either a great benefit or a large impediment to using AM effectively (depending on the needs and expertise of the user). Some work has been done to find ways to leverage this and the internal residual stresses^{9–14} to improve and tailor the materials, but until the phenomenon for AM is better understood and controllable, it is

¹Department of Industrial and Enterprise Systems Engineering, University of Illinois at Urbana–Champaign, Urbana, IL, USA

²Department of Industrial & Systems Engineering and Engineering Management, University of Alabama in Huntsville, Huntsville, AL, USA

³Department of Production Engineering, Federal University of Paraná, Curitiba, Paraná, Brazil

Corresponding author:

Albert E. Patterson, University of Illinois at Urbana–Champaign, 117 Transportation Building, 104 South Mathews Ave, Urbana, IL 61801, USA.

Email: ptttrsnv2@illinois.edu

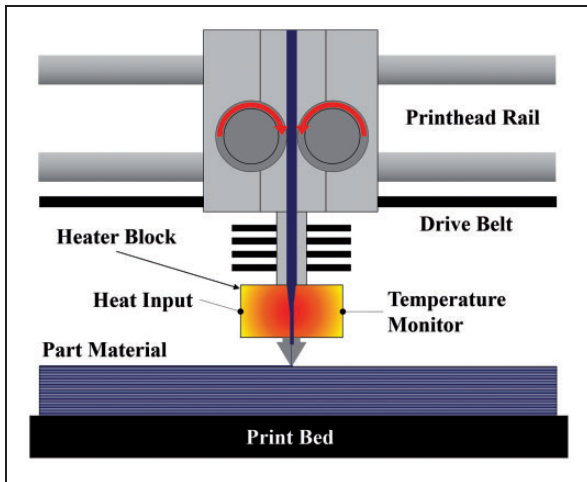


Figure 1. Fused deposition modeling (FDM) process (from Messimer et al.¹⁹ used with permission).

typically considered a disadvantage of using AM. This must be contemplated carefully during the process- and material-selection phases of product design. Significant work has been done to characterize the properties of AM materials,^{3,15–18} but aspects remain uncertain, particularly with respect to the dynamic and fracture behavior.

The most common AM process for polymer materials is the fused deposition modeling (FDM) process¹⁹ (Figure 1). This is an extrusion-based process which deposits molten filament in layers to build the part²⁰; the fusion between layers is accomplished via polymerization reaction between the layers. The materials produced by FDM are highly anisotropic, primarily due to the layering method which involve the production of *shell* and *infill* regions for each layer. As shown in Figure 2, the shell region is effectively the outer skin of the part, while the infill is the internal core. The infill pattern can vary^{21,22} depending on the desire of the user, but the most common configuration is the rectilinear pattern shown. There are a number of parameters that can be specified to produce enhanced combinations of properties for specific materials. The most important of these tunable parameters for an FDM material mesostructure are shown in Figure 2(a); other important considerations are the layer thickness and the printing parameters (such as printing speed, extrusion temperature, and similar inputs) themselves. All of these, in theory, can be designed and optimized according to the needs and wishes of the user.

Many studies^{3,23–29} on FDM materials relate mainly to the characterization of hollow or sub-full density parts, but the most useful case in practice is the full density case; here, the air gaps are set to zero or a negative value and the infill pattern completely fills the shell-enclosed region. Figure 2(c) shows manufactured examples of a rectilinear-infill, full density FDM material mesostructure with different

raster angles. The material shown is transparent high-temperature (MakerGeeks Raptor) polylactic acid (PLA). It is assumed that any remaining residual porosity in the full-density samples (per cross-sectional unit area) is homogeneous for a particular raster angle, regardless of the print orientation.^{7,8,30,31} Some work in functionally graded (non-homogeneous) materials has been done, but those are created intentionally and not a consequence of the FDM process mechanics.

Due to the extrusion-based layering technique used in FDM, it is possible to control the mesostructure pattern via the g-code generated for the printer to build the material; this level of control over process parameters and printing pattern possibility of using FDM to construct layer-based tailored polymer materials. However, most previous studies have focused on the macro-scale properties, so the influence of the mesostructure on the properties, particularly on the fracture properties, does not yet have an extensive literature. Recent work^{7,8,31–33} has begun to explore this influence for static testing and modeling, but the influence on the fracture behavior in these materials is not yet well understood.

An effective way to begin to explore the influence of this mesostructure on the fracture behavior of tailored FDM materials is to subject these materials to impact testing. One of the most common standard impact testing methods is the IZOD test^{34–36}; both the IZOD and the Tvergaard and Needleman³⁷ test have been well developed for testing materials, but the IZOD test has been shown to be generally preferable for testing polymer-based materials.^{34,38,39} Impact tests are very useful for understanding the basic fracture mechanics of a material, as they measure the amount of energy that is absorbed by a material during high-strain rate conditions before failure. The test studies the ductile–brittle transition of the material^{40–42}; this can be thought of as the total amount of energy required to initiate a fracture in the material from impact and propagate it through the full length of the material in one cycle.^{35,36} Clearly, much more work will need to be done to fully understand the crack behavior in FDM materials, but an impact test is a quick initial way to get reasonably accurate comparative results between materials and orientations. This allows the generation of a large dataset at a reasonable cost, which can be used to drive product design decisions and guide future research into the fracture behavior of these materials.

Impact testing has been performed previously on several FDM-processed materials,^{43–48} but a detailed look at the effect of the mesostructure pattern itself was not the focus of these studies. Only a small number of materials and samples were examined and in the context of macroscale analysis. For the influence of this mesostructure to be examined rigorously, it is necessary to consider the influence of both

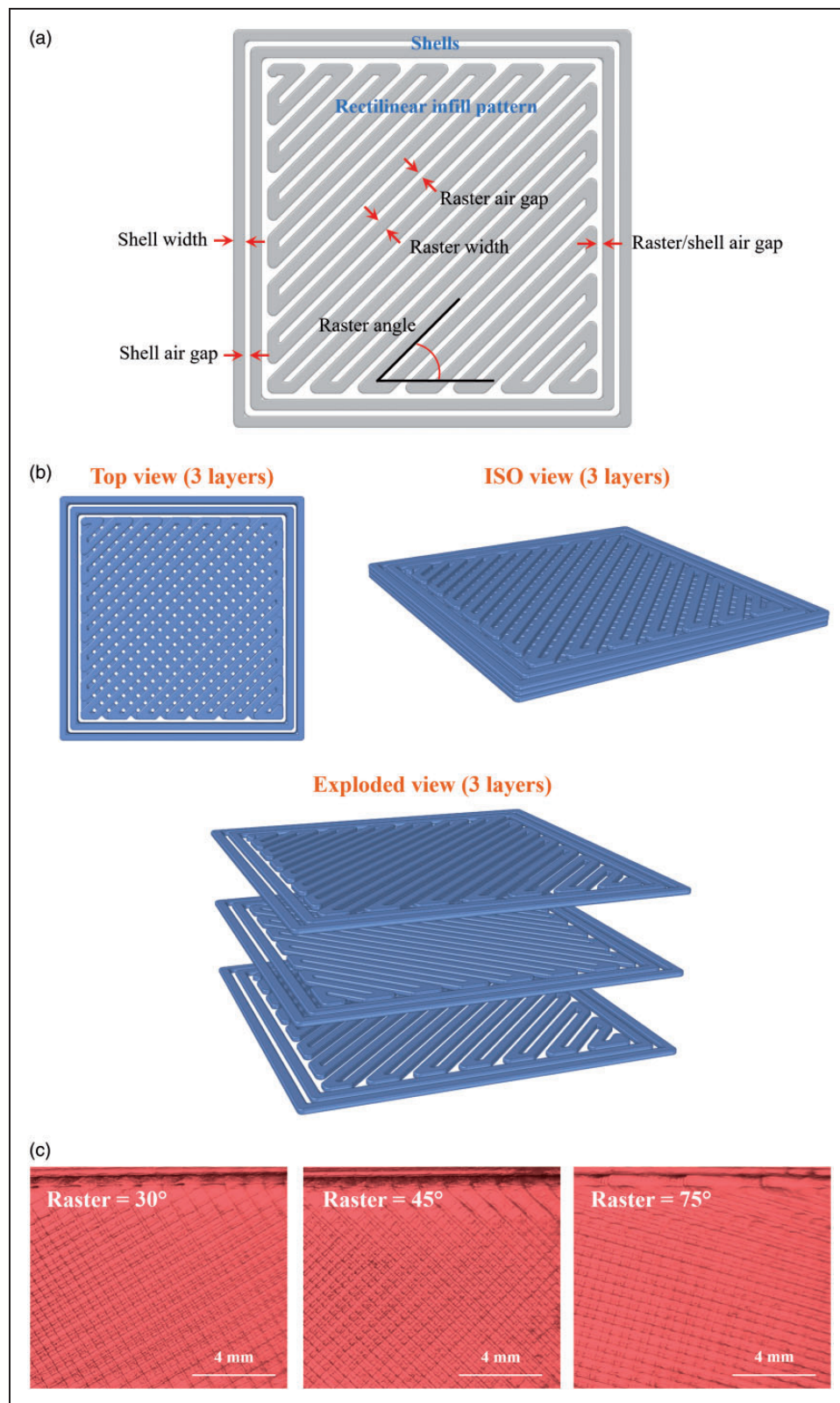


Figure 2. (a) Rectilinear layer structure, (b) configuration of several layers for FDM materials, and (c) manufactured examples (using transparent PLA with light behind).

the shell and the orientation of the raster lines in the print. In the present study, this was examined using a Type-E (reversed-notch) IZOD impact test based on ASTM D256. A standard shell was used in three

different orientations relative to the break angle, as well seven different hatch orientations. Ten different materials were tested, for a total of 210 different sample combinations; the tests were replicated five

times each, as required by ASTM D256, for a total of 1050 tests. The major contributions of the present study to the AM literature are:

- Presentation of a large impact resistance and impact energy dataset for multiple FDM materials
- Examination, explanation, and setup of the reversed-notch IZOD test for FDM polymer materials, which the authors recommend for testing FDM materials
- Detailed explanation of a feasible setup and conditioning method for FDM IZOD samples
- Comparison of 10 different materials under the same experimental conditions
- Examination of the influence of the shell and raster angle on impact strength in several combinations
- Discussion of the implications of the results in the context of fracture mechanics, materials design, and manufacturing.

Materials under study

The present work examined 10 distinct materials, tested using seven different hatch angles and three print orientations. As shown in Table 1, seven different pure materials were tested, as well as three composites; these were acrylonitrile butadiene styrene (ABS), standard PLA, high-temperature PLA, high-impact polystyrene (HIPS), nylon, polyethylene terephthalate + glycol (PETG), polycarbonate (PC), aluminum PLA, wood PLA, and carbon-fiber PLA. The most commonly printed FDM materials are ABS, PLA, and PETG, with nylon and PC also being relatively common. HIPS is not a common material for printing and is most commonly used as a support material, but it is a useful material on its own. High-temperature PLA is similar to standard PLA, except that the polymerization temperature is higher than simple PLA by 20%. Typical (filament manufacturer-defined) mechanical properties of the materials (excluding composites and high-temperature PLA (HTPLA)) used here are shown in Section S2 of the supplemental materials.

The three composite materials under study were made from PLA matrices with 40% fine aluminum powder, 40% wood fibers, and 15% chopped carbon fibers, respectively. This set of materials covers the most commonly used open-source materials for FDM with a wide range (200–260 °C) of processing temperatures. All of the used filaments (described in Tables 1 and 2) were standard open-source (nonproprietary) filament with available data sheets and which the authors were experienced in using. Proprietary materials were not used because the compositions are sometimes unknown, often containing additives or custom polymerization processes to be optimized for specific brands of FDM machines.

Table 1. Materials under study.

1	ABS	Acrylonitrile butadiene styrene
2	PLA	Polylactic acid
3	HTPLA	High-temperature PLA
4	HIPS	High-impact polystyrene
5	Nylon	Synthetic polyamide
6	PETG	Polyethylene terephthalate + glycol
7	PC	Polycarbonate
8	ALPLA	PLA + aluminum powder
9	WPLA	PLA + wood fiber
10	CFPLA	PLA + chopped carbon fiber

In order to test the effect of the shell and raster angle on the impact properties of the materials under consideration, it was necessary to vary these parameters. To this end, the three fundamental printing orientations were used, as shown in Figure 3: namely, the flat, horizontal, and vertical cases. The purpose of this was to explore the effect of the shell, as the different orientations had different shell/infill ratios when viewed in terms of each slice normal to the build plate (noting the pattern shown previously in Figure 2(a)). In the flat case, the shell was estimated to occupy about 5% of the total area for each layer, while the horizontal and vertical cases occupied about 20% and 50%, respectively. Note that these estimates are based on the standard ASTM IZOD dimensions,³⁴ a sample thickness of 3.25 mm, and extruder size of 0.40 mm. To vary the infill pattern in a controllable way, a standard rectilinear pattern was used. A sweep of 90° was done with the pattern in 15° increments. Figure 3(b) shows the sweep patterns for the seven angles; note that the angle shown is for the initial layer and that each subsequent layer was positioned 90° from the previous one. Refer to Figure 2(b) for a more detailed presentation of the concept.

Sample preparation

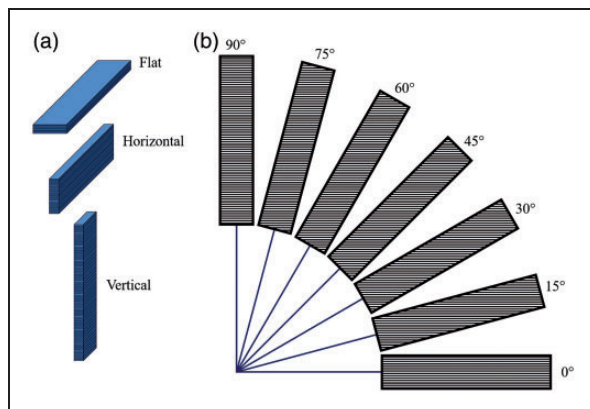
Design and manufacturing

The samples were manufactured using FDM, following the parameters shown in Table 2. Figure 4 shows the specimen configuration, while the first four columns of Table 3 show the dimensions of the final samples. These dimensions are well within the required specifications for samples from the ASTM standard.³⁴ Due to the potential for shrinkage or dimensional errors when processing the FDM materials (some of which have not yet been characterized well in the literature), it was decided to establish a nominal sample thickness of 3.25 mm. This allowed some shrinkage, while ensuring that all samples are at least 3.00 mm thick as required by the ASTM standard. Rectangular (instead of square) cross-section samples were used as this is the most common

Table 2. Sample manufacturing parameters.

Material	Samples	v (mm/s)	T_E ($^{\circ}\text{C}$)	T_B ($^{\circ}\text{C}$)	Base	Nozzle	Environment	Raw filament
ABS	105	50	225	90	Raft	Brass	Enclosed	Hatchbox pantone blue
PLA	105	60	200	50	Raft	Steel	Open	Hatchbox black
HTPLA	105	60	245	50	Raft	Steel	Open	MakerGeeks green raptor
HIPS	105	60	240	90	Raft	Brass	Enclosed	Monoprice premium (natural)
Nylon	105	50	250	70	Raft	Brass	Enclosed	eSUN ePA (natural)
PETG	105	60	240	80	Raft	Steel	Open	Inland white
PC	105	30	260	90	Raft	Brass	Enclosed	eSUN black
ALPLA	105	60	200	50	Raft	Steel	Open	SainSmart aluminum
WPLA	105	60	210	50	Raft	Steel	Open	Hatchbox wood
CFPLA	105	40	200	50	Raft	Steel	Open	3D Solutech carbon fiber

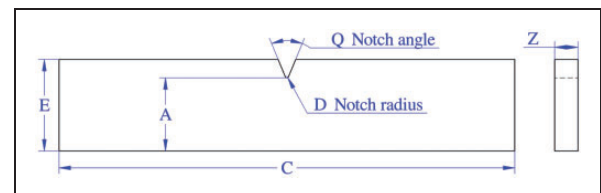
ABS: acrylonitrile butadiene styrene; PLA: polylactic acid; HTPLA: high-temperature PLA; HIPS: high-impact polystyrene; PETG: polyethylene terephthalate + glycol; PC: polycarbonate; ALPLA: PLA + aluminum powder; CFPLA: PLA + chopped carbon fiber; WPLA: PLA + wood fiber.

**Figure 3.** (a) Printing orientations and (b) raster angles.

configuration and the one most often shown in the testing literature. The precautions taken to prevent bending and buckling of the samples during the test will be discussed in a later section. The true thickness of each of the 1050 tested samples was recorded and used to calculate the impact resistance and impact energy at the level of each sample.

Due to the properties and behavior of the materials, it was necessary to print the ABS, HIPS, nylon, PETG, and PC inside of an enclosure. This necessitated the use of two printers built by the authors for research purposes, one with an enclosure and a Z-motion printbed and the other a Prusa-type printer. The Prusa-type machine was used to process the PLA, PETG, and PLA composites. Both printers used PC or glass printbeds,¹⁹ cooling fans, Bowden extruders, and aluminum frames for stability and were well constrained to prevent environmental vibrations. The belts, extrusion components, and some bearings were replaced before manufacturing the samples to prevent vibration and mechanical compliance effects in the samples.

Samples were printed in batches of 21 according to the parameters shown in Table 2. Each batch consisted of one sample of each parameter combination,

**Figure 4.** Specimen configuration (per ASTM D256).

ensuring that the statistical error analysis of the data would not be distorted and the repeatability between batches could be observed in the dataset. Printing order and configuration was the same as another published study by Messimer et al.⁴⁹ on the dimensional accuracy of FDM parts using most of the same materials and the same ASTM D256 sample geometry. That study should be consulted for a detailed description of the approach and assumptions followed for manufacturing of this type of specimens.

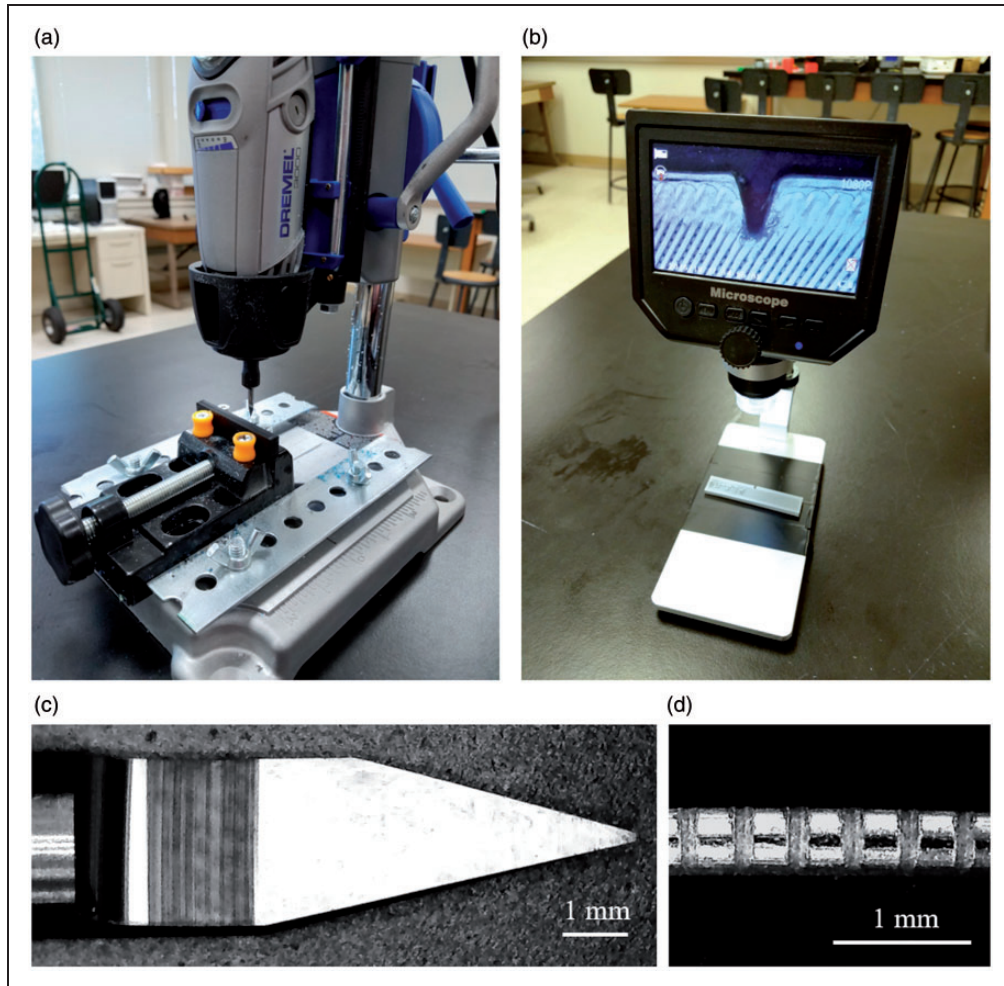
Several spare batches of samples were made as well, in case of a failure during testing, as allowed by the ASTM standard.³⁴ All filament rolls were conditioned before printing; all materials except nylon were kept in an air-conditioned ambient environment at approximately 23°C and 47% relative humidity for two weeks before printing. The nylon was kept in a sealed container with silica gel until shortly before printing, at which time it was placed in a dehydrator at 60°C until printing time. This dehydration was repeated each 24 h until the nylon samples were complete. The completed samples for all materials were allowed to rest in the ambient environment two to four weeks before notching to condition them and allow residual stresses to be released naturally from the material.

Notching

Several different notching methods for the FDM parts were attempted during the initial work on this experiment, including with a milling machine, router, and

Table 3. Sample dimensions and experimental conditions ($n = 1050$ for A, Z, C, and E and $n = 10$ for temperature and humidity).

	A (mm)		Z (mm)		C (mm)		E (mm)		Temperature ($^{\circ}\text{C}$)		Humidity (%)	
	Mean	[SD]	Mean	[SD]	Mean	[SD]	Mean	[SD]	Mean	[SD]	Mean	[SD]
Observed	10.16	[0.01]	3.28	[0.08]	63.50	[0.28]	12.72	[0.14]	22.17	[0.81]	51.00	[2.75]
Nominal	10.16 ± 0.05		3.25		63.50 ± 2.00		12.70 ± 0.20		23.00 ± 2.00		50.00 ± 10.00	

**Figure 5.** (a) Notcher, (b) inspection station, (c) main notch cutter, and (d) notch rounding file.

with a file. All of these methods were observed to severely damage the samples, making them unreliable for testing and out-of-spec from the requirement of the ASTM standard. The notches in previous literature on FDM materials did not focus on a feasible method for generating reliable and consistent notches, so there is not a standard method that has been established for FDM materials.

Because of a lack of a standard method for notching FDM samples that does not destroy the notches, a custom method was developed by the authors which proved to be effective. Figure 5(a) shows the tool built for this purpose, which uses a strong stand and rotary tool with a 0.25 mm tip 45° steel engraving bit (Figure 5(c)) to make the basic notches in a vertical

configuration. The function was similar to a miniature high-speed milling machine with a clamp that slid only in the Y-axis to ensure that the samples were held securely during the notching process. The steel engraving tool was very sharp and rotated at a speed of 35,000 r/min, allowing a very fast notch cut and no observed sample damage due to melting or chipping when checked using a microscope. In order to make the notches conform to the requirements of the ASTM standard, a final finishing of each notch was done using a 0.5 mm guitar bridge file (Figure 5(d)). Note that each sample was notched using a backing block.

A microscopic inspection station (Figure 5(b)) was used to ensure that the notches were good quality; each sample was checked, even though the ASTM

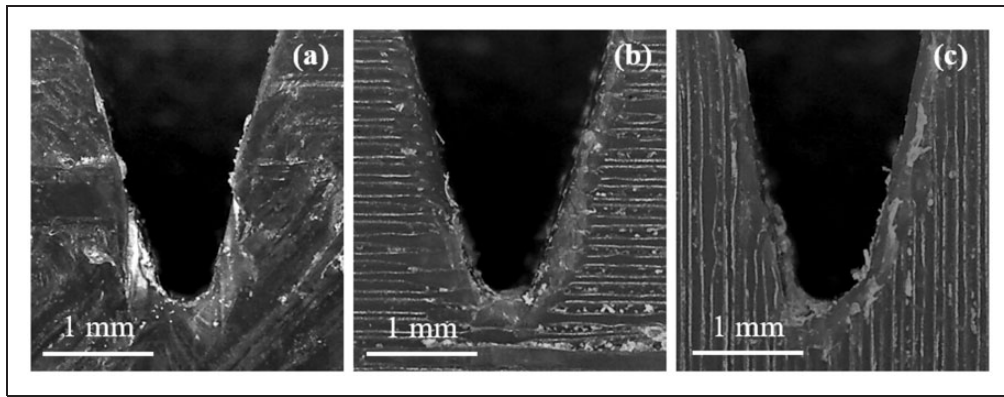


Figure 6. Example notches in (a) flat, (b) horizontal, and (c) vertical orientations.

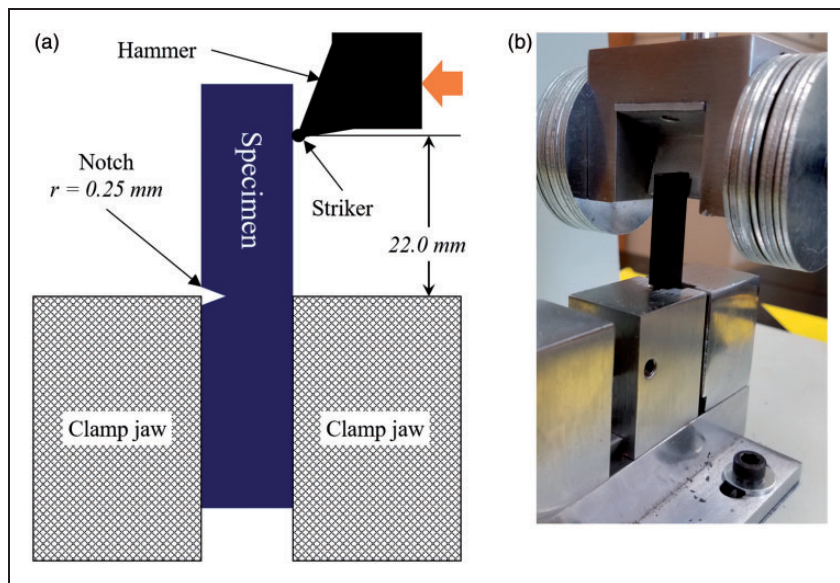


Figure 7. ASTM Type E IZOD machine/sample setup (a) diagram and (b) hardware.

standard only requires checking each 500 samples.³⁴ Figure 6 shows microscope images of the notches made for each print orientation.

Conditioning

As required by the standard, the samples were conditioned in an ambient environment after notching for 48–60 h before impact testing. Table 3 shows the conditions for both the sample curing and the testing. Note that, similarly to the conditioning of the filament, the nylon samples were kept in a dehydrator for approximately 40 h before notching and again before testing. A set of the final samples before testing can be seen in Section 1 of the supplemental materials.

IZOD testing

Experimental setup

The impact test chosen to be performed on the materials previously described was the ASTM D256 Type E

test, which used a reversed notch (Figure 7(a)). This is one of the four standard IZOD tests described in the ASTM standard³⁴ and the one that was anticipated to provide both the most consistent tests and the best comparative information for the influence of the shell. Often, un-notched tests are used to study highly anisotropic materials,^{50–52} but it was found during preliminary tests that the un-notched samples did not behave consistently for several of the materials. The preliminary work consisted of manufacturing several samples of each material (including notching and conditioning) for each orientation (raster angles of 0° and 90°) and running mock IZOD tests using them. None of the preliminary test samples were counted as true data points and were used only to tune and test the IZOD machine; the true specimens were much more carefully manufactured in batches, as described in the previous section. It was clear from the preliminary work that a stress concentrator was necessary to gain consistent results and reliable sample breaks; the type E test provided the ability to test the influence of the part shell, as well as the infill.

Table 4. Friction and windage correction input values.

Variable		Value
E_M	Pendulum energy (J)	2.7
h_M	Pendulum mass height at start (m)	0.600
L	Length of pendulum (m)	0.322
θ	Starting angle (°)	150.0
α_1	Angle for E_A (°) (mean [SD])	143.9 [0.57]
E_A	Energy lost through friction (J)	0.0153
β_1	Angle for E_B (°) (mean [SD])	145.3 [0.48]
E_B	Energy lost through windage (J)	0.0008

Preparation

Machine calibration. A simple pendulum-dial IZOD machine from ASR Instruments was used for the experiments. Before the tests, the machine was completely refurbished, during which all of the bearings and essential fasteners were replaced and the provided weights were replaced using ones that were calibrated by the authors to ensure accuracy. The dial assembly for the machine was also rebuilt and carefully tuned. The machine was oiled every 30 impact tests and checked for calibration after each material (105 samples). Pointer calibration and error measurement were done according to Section 10.3 of ASTM D256.³⁴ This was done at the beginning of the tests and repeated after each material to insure that the machine remained calibrated. It was found that the pointer energy loss was consistent throughout the test series at approximately 1.11% with the small 2.7J pendulum, which will be accounted for in the friction and windage correction factor calculated later.

Friction and windage correction. Per the ASTM D256 standard,³⁴ a correction factor was calculated to determine the effects of friction and windage on the experimental results. A single factor cannot be calculated for the whole experiment and must be calculated for each sample. As described in the previous sections, careful calibration of the machine was done before any tests were completed, so the friction and windage effect is inherent in the machine design and not due to wear or degradation of the machine. The values called for in Section A2 of the ASTM D256 standard are shown in Table 4; the values are the mean and standard deviation of 10 runs with the freshly calibrated machine.

Clearly, the energy lost from the friction and windage is very small but they are still worth considering in this experiment to ensure the most accurate data possible. Per the standard,³⁴ these values can be used to calculate the correction energies for each specimen. The maximum angle β_{max} of one swing was measured from the machine as the value of $\alpha_1 = 143.9^\circ$ in Table 4.

For each sample, the angle β_{sample} is measured and used to calculate the uncorrected

energy E_S . For each reading, the total correction energy is

$$E_{TC} = \left(E_A - \left(\frac{E_B}{2} \right) \right) \left(\frac{\beta_{sample}}{\beta_{max}} \right) + \left(\frac{E_B}{2} \right) \quad (1)$$

The impact resistance for each sample is calculated as

$$I_R = \frac{E_S - E_{TC}}{t} \quad (2)$$

where t is the sample thickness. Similarly, the impact energy is calculated to be

$$I_E = \frac{E_S - E_{TC}}{At} \quad (3)$$

where t is the sample thickness and A is the thickness of material under the notch.

Sample clamping and measurement

Measurement of the samples was completed using a pair of digital vernier calipers with a resolution of 0.01 mm, using the microscopic inspection station to verify notch depth as needed. The samples were clamped into the IZOD machine, (see Figure 7(b) for the hardware setup) taking extreme care to ensure that they were straight and correctly aligned. The notch was positioned using a thin, flat blade to ensure that it was positioned correctly relative to the clamp; the blade was blunted and positioning was done very carefully to prevent notch damage from the blade. Clamping was done only finger-tight to provide a secure base for the sample while providing consistent clamping pressure.

Procedure

For each sample, the pendulum was raised, latched, and clamped (for safety) with the raised position being set at an angle of 150° via an adjustable latch. The pendulum was then released and allowed to strike the sample. The final position of the pendulum was recorded at a resolution of 0.5° . Any samples that were observed to twist or buckle (observed to be only 0.6% of samples for the present study) were thrown out and repeated with fresh samples. A 2.7J pendulum was used, requiring a minimum of 15% energy remaining at the end of a test; this was an appropriate energy level for all materials, with the most energy absorbed by a sample observed to be 71% of the pendulum energy.

Results

A summary of the results by material and print orientation is shown in Table 5. This set shows the average

Table 5. Summary of mean experimental results by material and orientation.

Material	Orientation	<i>n</i>	<i>I_R</i> (J/m)	<i>I_E</i> (J/m ²)
ABS	Flat	35	128.69	12,558
ABS	Horizontal	35	149.14	14,670
ABS	Vertical	35	55.14	5427
PLA	Flat	35	152.52	15,008
PLA	Horizontal	35	113.21	11,137
PLA	Vertical	35	77.42	7619
HTPLA	Flat	35	139.70	13,745
HTPLA	Horizontal	35	98.67	9709
HTPLA	Vertical	35	87.77	8639
HIPS	Flat	35	143.25	14,106
HIPS	Horizontal	35	151.07	14,864
HIPS	Vertical	35	45.30	4458
Nylon	Flat	35	324.90	31,974
Nylon	Horizontal	35	248.86	24,484
Nylon	Vertical	35	59.61	5864
PETG	Flat	35	238.98	23,525
PETG	Horizontal	35	178.09	17,531
PETG	Vertical	35	35.45	3489
PC	Flat	35	354.15	34,851
PC	Horizontal	35	514.90	50,689
PC	Vertical	35	42.03	4138
ALPLA	Flat	35	93.11	9165
ALPLA	Horizontal	35	85.90	8451
ALPLA	Vertical	35	48.93	4814
CFPLA	Flat	35	79.34	7810
CFPLA	Horizontal	35	80.45	7917
CFPLA	Vertical	35	41.17	4052
WPLA	Flat	35	124.29	12,234
WPLA	Horizontal	35	99.93	9835
WPLA	Vertical	35	29.46	2900

ABS: acrylonitrile butadiene styrene; PLA: polylactic acid; HTPLA: high-temperature PLA; HIPS: high-impact polystyrene; PETG: polyethylene terephthalate + glycol; PC: polycarbonate; ALPLA: PLA + aluminum powder; CFPLA: PLA + chopped carbon fiber; WPLA: PLA + wood fiber.

for each material and print orientation to give a “nominal” comparison, as raster angle is not typically considered (or fixed at one or two settings) for impact testing of polymer materials. The full data set (orientation and raster angle) for the impact resistance and impact energy is shown in Figures 8 and 9, respectively. The coefficient of variation was calculated as well and is shown in Figure 10.

Note that the general shapes for the two sets are similar, but they are not exact scales of each other due to small variations of the notch depth for each sample; this was measured and calculated for each individual sample. The full dataset is too long to tabulate here, so it is given in Section S4 of the supplemental materials.

Discussion

The mission of the present study was to explore the effects of the printing orientation, and the raster angle on the impact resistance and impact energy on a set of common FDM polymers. The set of polymers to test was selected based on their usefulness for FDM applications and their ability to be subjected to impact testing. Some additional FDM materials were explored initially, particularly thermoplastic polyurethane (TPU), polyvinyl alcohol (PVA), and high-density polyethylene (HDPE), but these were found to be too soft and unsuitable for impact testing during a series of qualifying trials.

The essential function of an impact test is to get a “general” measure of the toughness or “fracture resistance” of a material by measuring the amount of energy required to break a sample⁵³ completely. IZOD is a bending-type impact test, where the metrics gathered are the amount of energy used to fully break a sample as a function of thickness (i.e., impact resistance) and as a function of the fractured cross-sectional area (i.e., impact energy). Essentially, the measured energy is the total energy required to initiate a crack in the sample and grow it for a length equal to the length of the sample (for fracture resistance) or initiate and grow a fracture equal in surface area to the sample’s cross-sectional area (in fracture energy). This method of measuring toughness can be considered to be a “bulk” method, as it gives the total energy dissipated in the material and does not allow the study of local fracture effects or the plastic deformation around the crack tip. However, it is a standardized, relatively simple, method that provided a well-understood metric; therefore, it is an appropriate test, especially for a large number of samples as in this study. From the information presented, a designer interested in better understanding the effects can use the IZOD data to select materials, orientation, and raster angles for an in-depth study using more precise techniques.

Since impact tests are a method for measuring the energy required to fracture a material, then three essential effects will determine impact properties: plastic deformation before crack initiation and during crack growth, crack length (for impact resistance) or crack surface area (for impact energy), and the ability for the material to absorb energy without deforming or fracturing. For the anisotropic FDM materials, all three are determined by both the material properties and the mesostructure of the material. The ASTM IZOD standard³⁴ defines four different types of tests available, from which the Type E test was selected for the present study. The mechanics of this test are shown in Figure 11; note that the notch is on the reverse side of the hammer strike. This type of test is particularly useful for FDM materials, as it allows the effect of the shell to be measured, instead of bypassed via the notch is another type of impact

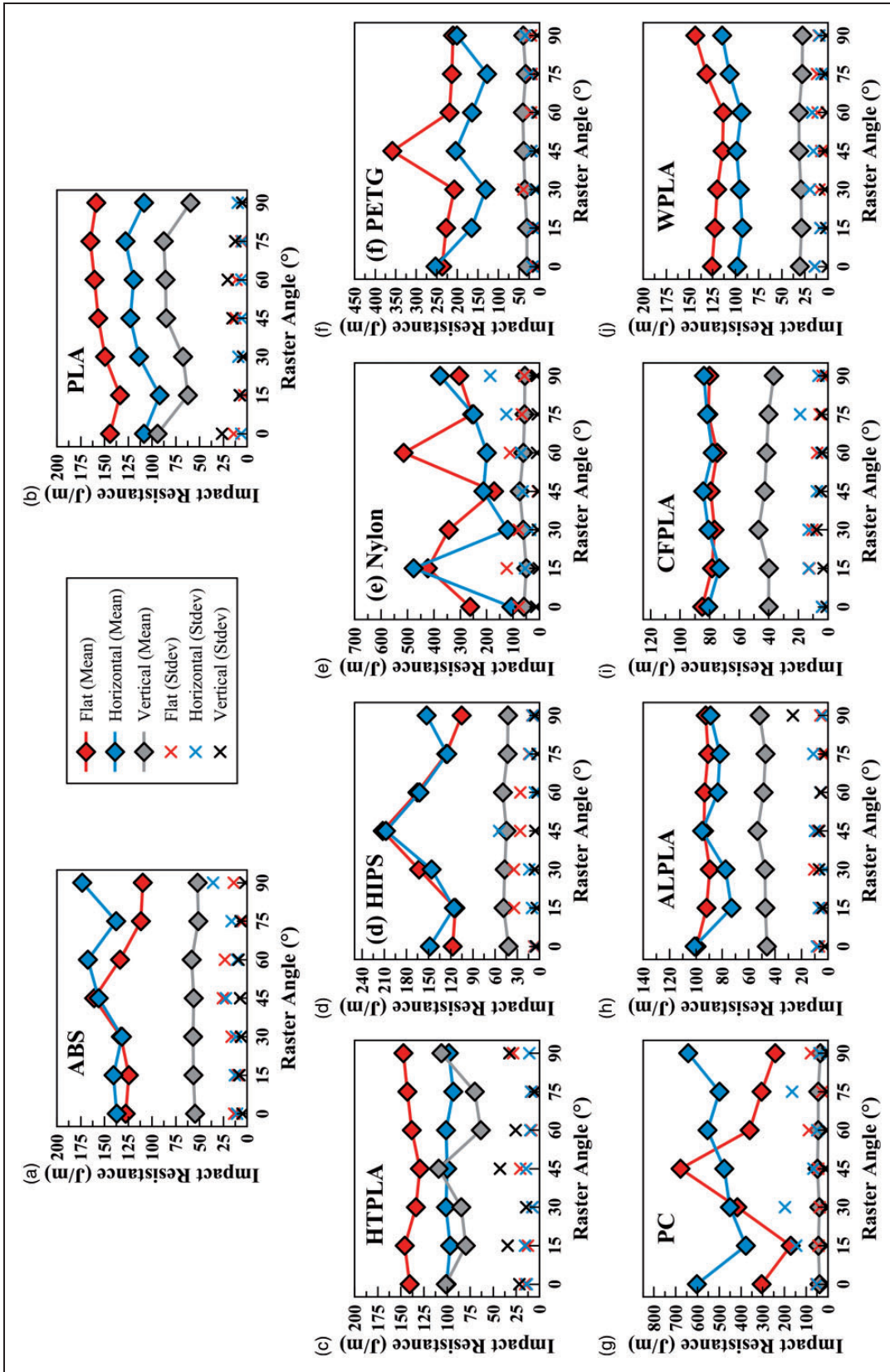


Figure 8. Measured impact resistance (J/m) mean and SD ($n = 5$) for (a) ABS, (b) PLA, (c) HTPLA, (d) HIPS, (e) nylon, (f) PETG, (g) PC, (h) ALPLA, (i) CFPLA, and (j) WPLA as function of orientation and raster angle.

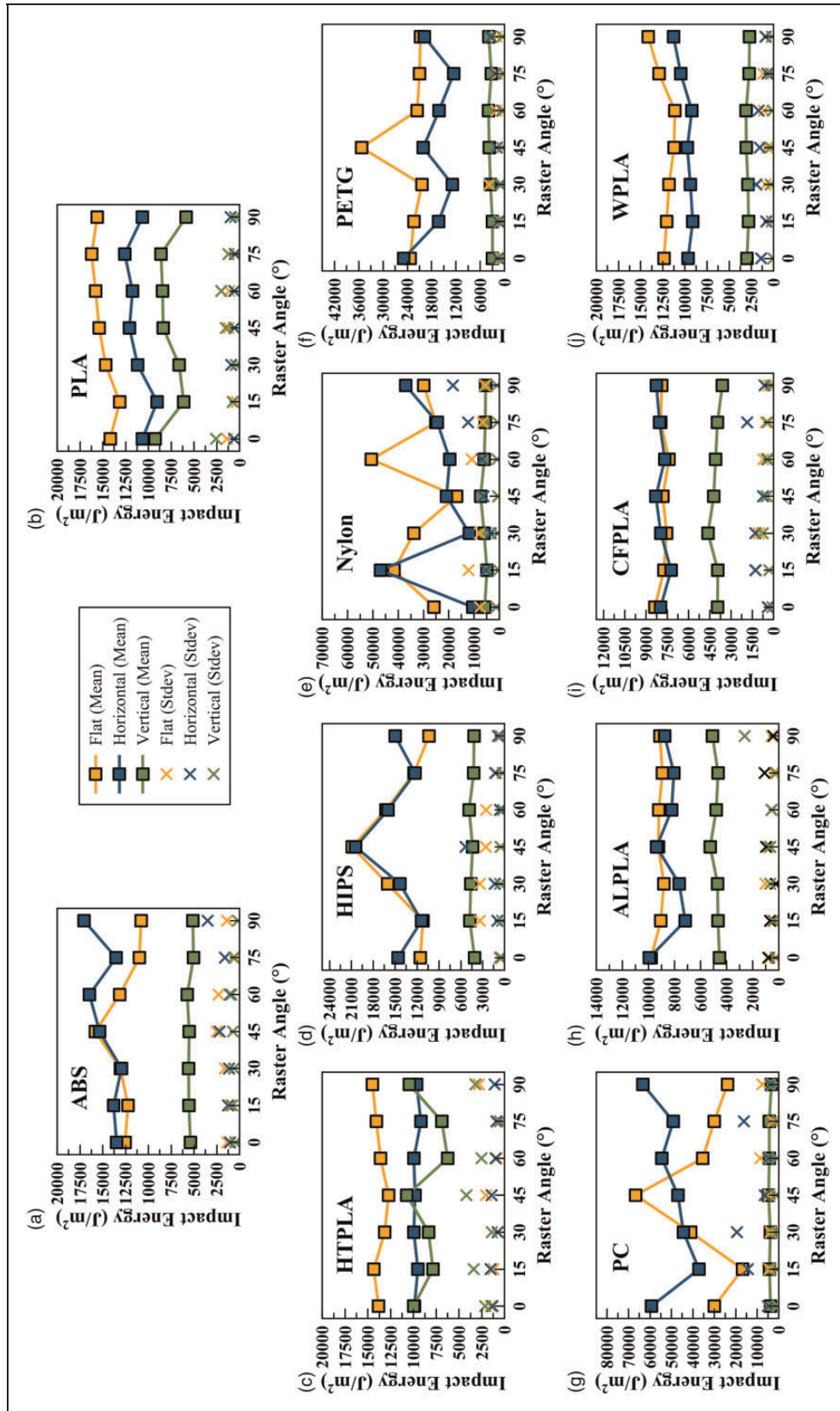


Figure 9. Measured impact energy (J/m^2) mean and SD ($n=5$) for (a) ABS, (b) PLA, (c) HTPLA, (d) HIPS, (e) nylon, (f) PETG, (g) PC, (h) ALPLA, (i) CFPLA, and (j) WPLA as function of orientation and raster angle.

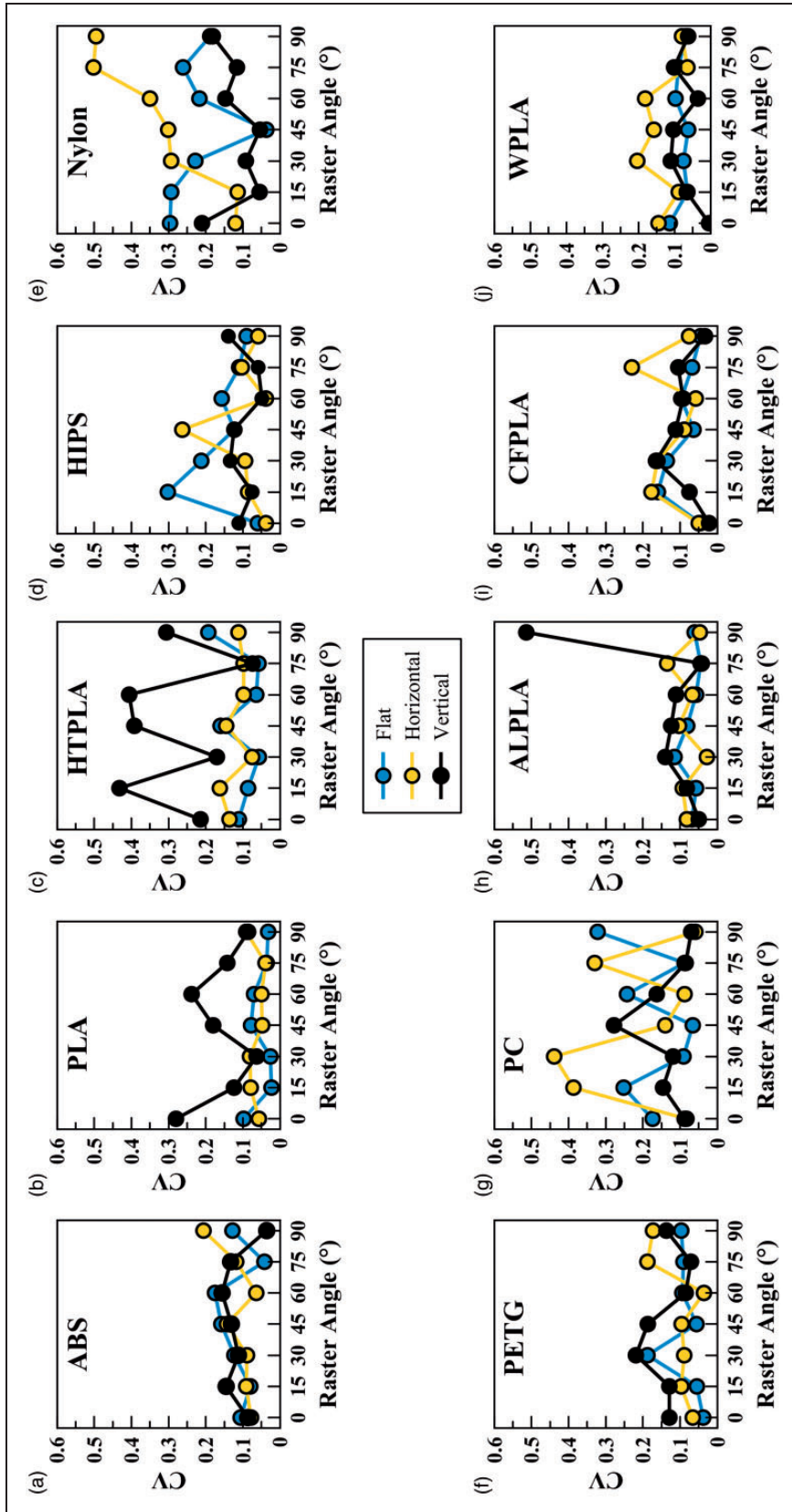


Figure 10. Coefficient of variation ($n = 5$) for (a) ABS, (b) PLA, (c) HTPLA, (d) HIPS, (e) nylon, (f) PETG, (g) PC, (h) ALPLA, (i) CFPLA, and (j) WPLA as function of orientation and raster angle.

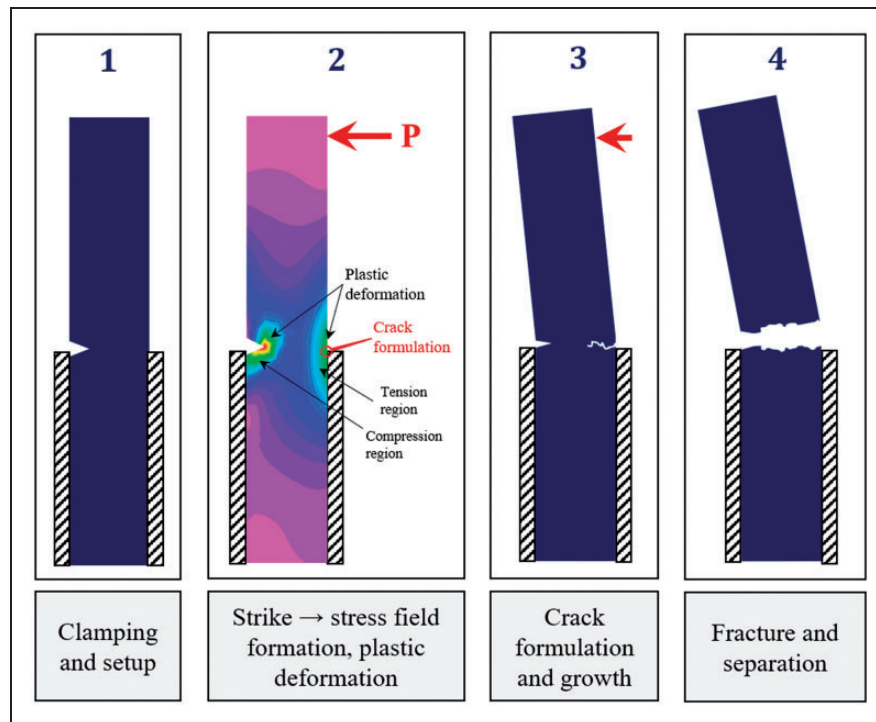


Figure 11. ASTM D256 IZOD Type-E test stress and fracture steps.

test. As shown, the hammer strike will begin the deformation of the shell and initiate a crack, which will then grow through the infill until it reaches the notch and the fracture is complete. In a real-world application, the shell would exist around the part and would influence the initiation of fractures in a similar way to this impact test.

This study analyzed the three standard FDM printing orientations, as shown in Figure 12, in order to capture the fracture behavior of all these cases. Note that the behavior described here was expected for the standard rectilinear pattern, but may be different for other kinds of infill patterns. In the case of the flat orientation (Figure 12(a)), the crack can be expected to form in the shell, which will then be influenced by the raster angle as it enters the infill region. The figure shows some experimental observations which do behave as predicted.

The infill pattern was expected to have a much smaller impact on the horizontal orientation (Figure 12(b)), but the experimental observations showed that it did indeed have an impact on the crack growth; it was observed that for this orientation, the fractures initiated at a point where a stress concentration existed in the infill pattern, as shown in the figure, and grew to the notch.

Finally, the vertical orientation (Figure 12(c)) was not expected show much or any influence from the infill, as the fracture is expected to follow the print layer boundary. However, it was observed that the main effect from the boundary was to create a random stress concentration to start the crack and that the notch position did not directly affect the

fracture in many of the cases. The raster angle seemed to influence the results somewhat, most likely due to differences in contact time and temperature during printing of each layer; the layer adhesion appeared to be the determining factor, so this is a logical conclusion from the observed behavior.

When these effects are taken into consideration, the results shown in Figures 8 and 9 can be better interpreted; essentially, the anisotropic structure of the materials directly influenced the crack length, which in turn was the primary driver of the energy tolerance of the material. The coefficient of variation, in this context, is a good measure of how consistent the crack growth and formulation is within a particular material angle orientation over the various experimental replications. For example, Figure 10 strongly suggests that ABS and PLA + wood fiber (WPLA) are quite consistent, while nylon and PC are quite non-consistent. Note, however, that the most brittle materials tended to be more consistent in general than the ductile ones. This suggests that local plastic deformation within the mesostructure could also be an important factor and one that was anticipated when examining the fracture surfaces.

In addition to the mesostructure, the main driver of the crack behavior was the behavior of the material itself. One of the fundamental assumptions made when modeling defined mesostructures is that the material within each grain or bead is isotropic and that the source of anisotropy is the arrangement of these isotropic elements. During the course of the testing, it was noted that the materials under study fell into one of three categories, based on their general

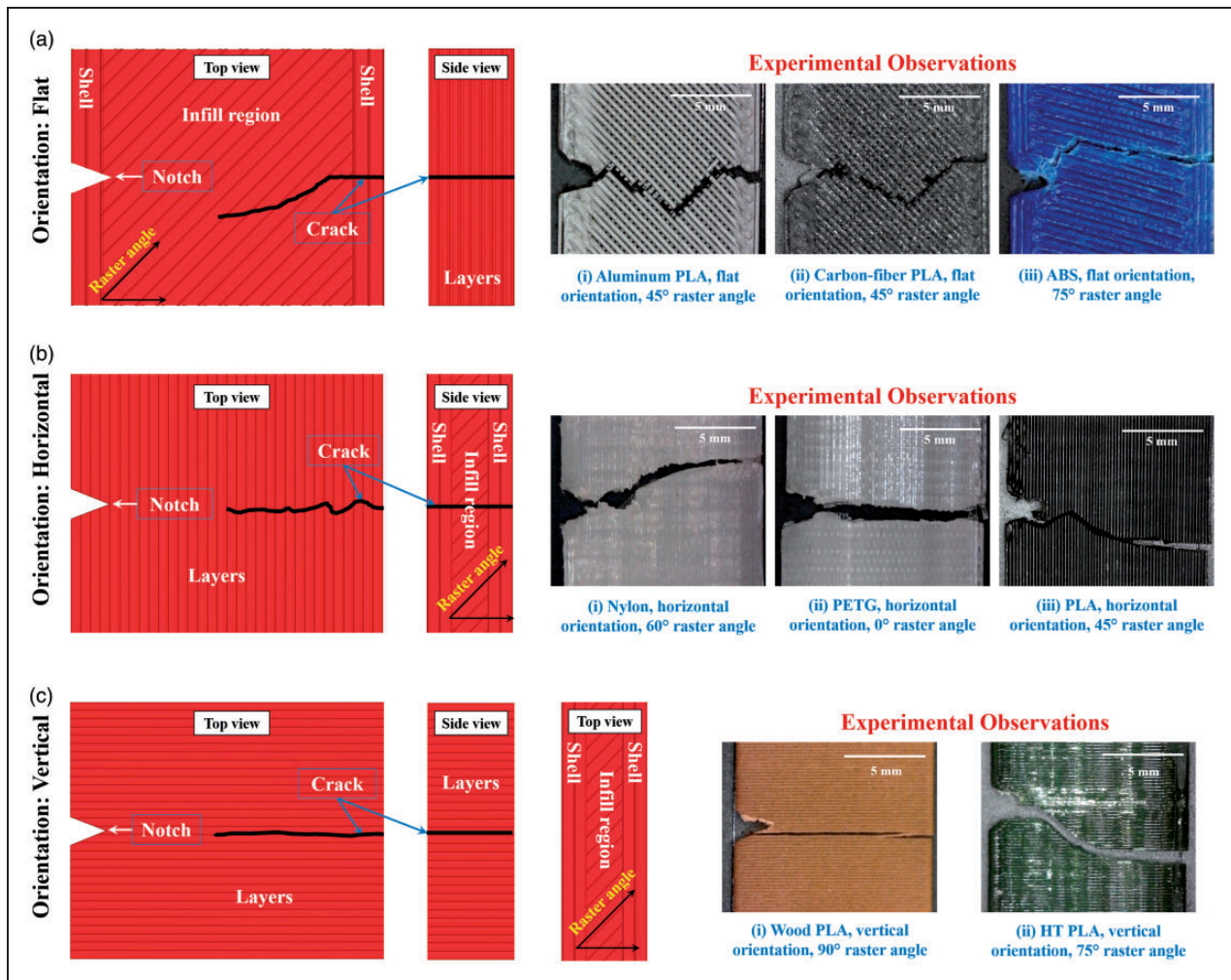


Figure 12. Impact of raster angle for (a) the flat orientation, (b) the horizontal, and (c) vertical orientation. Also given are experimental observations which confirm the models shown.

behavior and not on the relative toughness: (1) brittle materials, (2) semi-plastic materials, and (3) plastic materials.

1. Brittle materials: These were the materials with a “clean” fracture after testing and that did not show much or any local plastic deformation when examined. In this study, these materials were PLA, WPLA, PLA + chopped carbon fiber (CFPLA), and PLA + aluminum powder (ALPLA).
2. Semi-plastic materials: These showed some plastic deformation in the fracture surface, but it was mostly localized and not very deep into the part. There was no layer pull-out or warping of the part during the test. These were found to be ABS, HTPLA, and HIPS.
3. Plastic materials: Finally, three of the materials (PC, nylon, and PETG) showed significant plastic deformation, including large and deep scars in the part, stretching, and layer pullout.

For each of these cases and for each orientation, optical microscope examinations were performed, as

shown in Figure 13. The brittle cases examined were CFPLA (flat, 30° raster angle) (Figure 13(a)), PLA (horizontal, 75°) (Figure 13(d)), and WPLA (vertical, 90°) (Figure 13(g)). In all of these cases, the crack surface is clean and does not show any signs of notable plastic deformation. This is due to the general brittleness of these materials, as well as the presence of voids (Figure 13, Note [A]) from poor layer adhesion in some areas. Since the same FDM machines and print trajectories were used for all materials and these voids were only observed in the brittle materials, it is reasonable to conclude that the issue is with the material flow behavior and not manufacturing process defects.

Next, the semi-plastic cases were analyzed; these were ABS (flat, 30°) (Figure 13(b)), HTPLA (horizontal, 60°) (Figure 13(e)), and HIPS (vertical, 60°) (Figure 13(h)). All three cases showed some local plastic deformation, but it was not serious, was mainly confined to the crack surface, and did not deform the parts themselves. Note that the HTPLA, unlike the PLA and PLA composites in the brittle set, did not show voids in the mesostructure. HTPLA has a

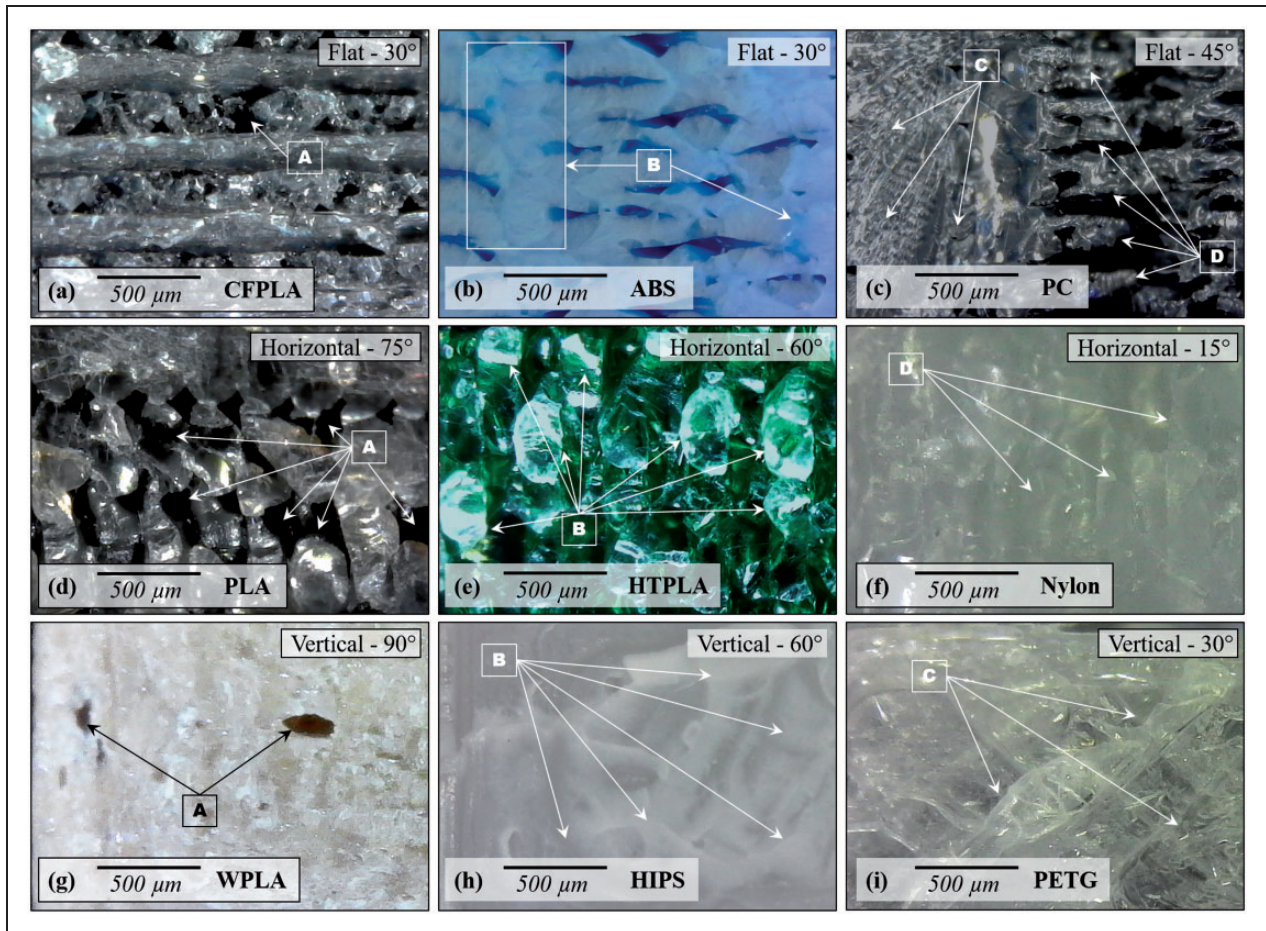


Figure 13. Example fracture surface microscope images for (a) CFPLA (brittle, flat), (b) ABS (semi-plastic, flat), (c) PC (plastic, flat), (d) PLA (brittle, horizontal), (e) HTPLA (semi-plastic, horizontal), (f) nylon (plastic, horizontal), (g) WPLA (brittle, vertical), (h) HIPS (semi-plastic, vertical), and (i) PETG (plastic, vertical). Note: [A] voids in material caused by test shock or poor layer adhesion of material, [B] local plastic deformation near surface, [C] deep plastic deformation, and [D] severe material stretching and layer pullout.

significantly higher polymerization temperature than standard PLA, suggesting the high-temperature version of the material has superior flow properties and layer adhesion.

Finally, the plastic materials were studied. These three, PC (flat, 45°) (Figure 13(c), nylon (horizontal, 15°) (Figure 13(f), and PETG (vertical, 30°) (Figure 13(i)), all showed strong signs of significant plastic deformation during the test. While the PETG showed severe plastic deformation at the crack site, it was relatively mild compared with the effect on the PC and nylon; these two materials were so plastically deformed at the crack that the entire part was deformed during the test. Figure 14 show examples of these from tested samples. Clearly, this was the source of the very high toughness for both materials, as well as the source for the relatively low consistency between runs. In spite of the deformation, all of the samples fractured as expected and followed the ASTM standard for the test, so they were accepted as valid data. The test³⁴ allows for any amount of plastic deformation as long as the sample can be fractured fully and tossed in one strike of the hammer.

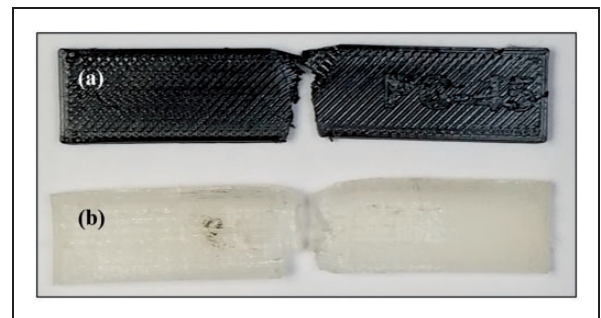


Figure 14. Macro-scale image of severe plastic deformation and layer pull-out for (a) PC and (b) nylon.

Some voids were present in the “brittle” materials (Figure 13) and not the others, so a brief exploratory study was done to find the difference in density between the three categories of materials. For each of the standard PLA (brittle), ABS (semi-plastic), and PC (plastic), 10 random samples left over from the tests were selected for a brief mass-density study. Note that these samples were un-notched and did not contain any markings or number designations, so they

were simple to measure in terms of their total volume. For each sample, the basic dimensions were measured, which was used to calculate the theoretical mass, based on manufacturer density values given in Section S2 of the supplemental materials. Each sample was then weighed with a jewelry scale with a resolution of 0.001 grams and the mass compared to the theoretical mass. This gave a good indication of the total volume of potential voids in the material; details and calculated values can be seen in Section S3 in the supplemental materials. It was found that the PLA had an average density of 93.74%, while the ABS and PC both had average densities of 99.21% but different standard deviations of this value; PC was more consistent than ABS over the samples surveyed. This is exactly the results expected after examining the microscope images in Figure 13. Further work is needed in this area to understand the presence of voids and local defects in FDM parts for these various materials and this mass-density approach appears to be effective and feasible.

One of the next steps to be completed for this work is to complete an analysis of variance (ANOVA) and correlation analyses between the various factors and parameters and the observed responses. This was not completed for this study, as it would be very extensive and will be presented in a follow-up stand-alone work. This is a full-order experiment, since all selected levels of the factor combinations were tested. The use of a full-order experiment allows more extensive and rigorous data analysis, including the analysis of the factor interactions. It is expected that the level of significance of the factors will vary from material-to-material, with the materials with the largest variance in response being more affected (e.g., HIPS, nylon, and PC). For the ANOVA, the experimental design consists of two main factors (orientation and raster angle) with three and seven levels, respectively, and three responses (fracture resistance, fracture energy, and coefficient of variation). The experiment had five replications, so the testing and validation of the Fisher assumptions (normality of residuals, equal variance between replications, and independence of residuals in run order) required for proof of ANOVA validity will not be difficult to accomplish.

In addition to factor and interaction significance, numerous correlations between the process parameters and material properties can be done using this dataset as well. This is also a topic of ongoing work, as the analysis and presentation are too extensive to present in this study and will be given in a later paper. For the parameter correlations, it is expected that the printing temperature will have a strong correlation with the toughness and consistency, but others may be influential as well. It is expected that this correlation analysis will be the seed for more extensive follow-up work in this area, most likely with smaller and more focused experiments.

Conclusions

Overall, this study provided a large amount of useful information and insight into the mechanics of anisotropic FDM parts. Important conclusions from the results are:

- Careful IZOD testing is an effective method for toughness testing of FDM materials based on the success of this study
- The shell orientation of the parts and the structure of the infill strongly affect the fracture properties of the material
- As predicted by fracture mechanics theory, the crack length and material plasticity were the primary drivers of the material impact toughness
- The raster angle was observed to “steer” the crack in a predictable way for the flat orientation and in a less-predictable way for the other two
- The Type-E IZOD test was effective, since it allowed the study of both the shell and infill on the material toughness
- Brittle FDM materials are more consistent in terms of impact properties but also generally weaker
- Materials that undergo large plastic deformation before fracturing are tougher, but more unpredictable in terms of impact properties
- The use of particulate additives within PLA (i.e. WPLA, CFPLA, and ALPLA) serves to reduce the toughness, while also reducing the degree of anisotropy.

Acknowledgements

The authors wish to thank the UAH ISEEM Department for providing laboratory space and raw materials used in the completion of this study. Thanks also to Daniel Herber for his extensive informal comments on this work and its presentation. All opinions and conclusions presented in this work are solely those of the authors; no external funding was used to produce, direct, or publish this work.

Supplemental material

Supplemental material for this article is available online which complement this manuscript and provides the full dataset used to drive the results and discussion sections. The supplement is divided into four section, each giving some important information:

- Section S1: An image of a set of completed specimens, where each orientation and material is represented.
- Section S2: A brief background study of the theoretical filament properties for the main materials used in this work (not including the composite materials nor HTPLA).
- Section S3: Describes the data and calculations for the brief mass-density analysis on the ABS, PLA, and PC samples, as discussed in Section 6.
- Section S4: The data set described in Figures 8 to 10.

Declaration of Conflicting Interests

The author(s) declared no potential conflicts of interest with respect to the research, authorship, and/or publication of this article.

Funding

The author(s) received no financial support for the research, authorship, and/or publication of this article.

ORCID iD

Albert E Patterson  <http://orcid.org/0000-0003-0849-1599>

References

1. ASTM. *ASTM F2792-12a: Standard terminology for additive manufacturing technologies*. West Conshohocken, PA: ASTM International, 2012.
2. Guo N and Leu MC. Additive manufacturing: technology, applications and research needs. *Front Mech Eng* 2013; 8: 215–243.
3. Ahn SH, Montero M, Odell D, et al. Anisotropic material properties of fused deposition modeling ABS. *Rapid Prototyping J* 2002; 8: 248–257.
4. Sood AK, Ohdar R and Mahapatra S. Parametric appraisal of mechanical property of fused deposition modelling processed parts. *Mater Design* 2010; 31: 287–295.
5. Kunze K, Etter T, Grässlin J, et al. Texture, anisotropy in microstructure and mechanical properties of IN738lc alloy processed by selective laser melting (SLM). *Mater Sci Eng A* 2015; 620: 213–222.
6. Hitzler L, Hirsch J, Heine B, et al. On the anisotropic mechanical properties of selective laser-melted stainless steel. *Materials* 2017; 10: 1136.
7. Alaimo G, Marconi S, Costato L, et al. Influence of meso-structure and chemical composition on FDM 3d-printed parts. *Compos Part B Eng* 2017; 113: 371–380.
8. Somireddy M and Czekanski A. Mechanical characterization of additively manufactured parts by FE modeling of mesostructure. *J Manufact Mater Process* 2017; 1: 18.
9. Yu HZ, Cross SR and Schuh CA. Mesostructure optimization in multi-material additive manufacturing: a theoretical perspective. *J Mater Sci* 2017; 52: 4288–4298.
10. Kalentic N, Boillat E, Peyre P, et al. Tailoring residual stress profile of selective laser melted parts by laser shock peening. *Additive Manufac* 2017; 16: 90–97.
11. Tammas-Williams S and Todd I. Design for additive manufacturing with site-specific properties in metals and alloys. *Scripta Materialia* 2017; 135: 105–110.
12. Garcia D, Jones ME, Zhu Y, et al. Mesoscale design of heterogeneous material systems in multi-material additive manufacturing. *J Mater Res* 2017; 33: 58–67.
13. Pei E and Loh GH. Future challenges in functionally graded additive manufacturing. In *Additive manufacturing—developments in training and education*. Springer International Publishing, 2018, pp.219–228.
14. Srivastava M, Rathee S, Maheshwari S, et al. Design and processing of functionally graded material: review and current status of research. In *3D Printing and additive manufacturing technologies*. Springer Singapore, 2018, pp.243–255.
15. Chua CK, Wong CH and Yeong WY. *Standards, Quality Control, and Measurement Sciences in 3-D printing and Additive Manufacturing*. London: Academic Press, Elsevier 2017, pp. 95–137.
16. Caputo D, Aprea P, Gargiulo N, et al. The role of materials and products characterization in the additive manufacturing industry. In: *2017 IEEE 3rd international forum on research and technologies for society and industry (RTSI)*. Modena, Italy, 11 September-13 September 2017. IEEE.
17. Dizon JRC, Espera AH, Chen Q, et al. Mechanical characterization of 3d-printed polymers. *Additive Manufac* 2018; 20: 44–67.
18. Patterson AE. Crack propagation in 3-D printed PLA: Finite element modeling, test bed design, and preliminary experimental results. Technical report, University of Illinois at Urbana-Champaign, Department of Industrial and Enterprise Systems Engineering, 2018, <http://hdl.handle.net/2142/100334> (accessed 4 September 2018).
19. Messimer SL, Patterson AE, Muna N, et al. Characterization and processing behavior of heated aluminum-polycarbonate composite build plates for the FDM additive manufacturing process. *J Manufac Mater Process* 2018; 2: 12.
20. Turner BN, Strong R and Gold SA. A review of melt extrusion additive manufacturing processes: I. process design and modeling. *Rapid Prototyping J* 2014; 20: 192–204.
21. Fernandez-Vicente M, Calle W, Ferrandiz S, et al. Effect of infill parameters on tensile mechanical behavior in desktop 3d printing. *3D Printing Additive Manufac* 2016; 3: 183–192.
22. Popescu D, Zapciu A, Amza C, et al. FDM process parameters influence over the mechanical properties of polymer specimens: a review. *Polymer Testing* 2018; 69: 157–166.
23. Aw YY, Yeoh CK, Idris MA, et al. Effect of printing parameters on tensile, dynamic mechanical, and thermoelectric properties of FDM 3d printed CABS/ZnO composites. *Materials* 2018; 11: 466.
24. Ang KC, Leong KF, Chua CK, et al. Investigation of the mechanical properties and porosity relationships in fused deposition modelling-fabricated porous structures. *Rapid Prototyping J* 2006; 12: 100–105.
25. Nuñez P, Rivas A, García-Plaza E, et al. Dimensional and surface texture characterization in fused deposition modelling (FDM) with ABS plus. *Procedia Eng* 2015; 132: 856–863.
26. Doubrovski Z, Verlinden JC and Geraedts JMP. Optimal design for additive manufacturing: opportunities and challenges. In: *Volume 9: 23rd International conference on design theory and methodology; 16th design for manufacturing and the life cycle conference*, Washington, DC, 28 August-31 August 2011, pp. 635–646. ASME.
27. Singh J, Singh R and Singh H. Repeatability of linear and radial dimension of ABS replicas fabricated by fused deposition modelling and chemical vapor smoothing process: a case study. *Measurement* 2016; 94: 5–11.
28. Zein I, Hutmacher DW, Tan KC, et al. Fused deposition modeling of novel scaffold architectures for tissue engineering applications. *Biomaterials* 2002; 23: 1169–1185.

29. Villalpando L, Eiliat H and Urbanic R. An optimization approach for components built by fused deposition modeling with parametric internal structures. *Procedia CIRP* 2014; 17: 800–805.
30. Huang B and Singamneni S. Raster angle mechanics in fused deposition modelling. *J Compos Mater* 2014; 49: 363–383.
31. Somireddy M, Czekanski A and Singh CV. Development of constitutive material model of 3d printed structure via FDM. *Mater Today Commun* 2018; 15: 143–152.
32. Delissen A, Radaelli G, Shaw LA, et al. Design of an isotropic metamaterial with constant stiffness and zero Poisson's ratio over large deformations. *J Mech Design* 2018; 140: 111405.
33. Spadaccini C, Jackson J, Watts S, et al. Integrated computational materials engineering (ICME) approaches to the design and fabrication of architected materials. In: *58th AIAA/ASCE/AHS/ASC structures, structural dynamics, and materials conference*, Grapevine, Texas, 9 January–13 January 2017, AIAA2017-1543.
34. ASTM. *ASTM D256-10e1: Standard test methods for determining the Izod pendulum impact resistance of plastics*. ASTM International, West Conshohocken, Pennsylvania, USA. 2018.
35. Slavin SE and Beswick GT. Instrumented izod impact testing. *J Appl Polym Sci* 1993; 49: 1065–1070.
36. Casiraghi T. The fracture mechanics of polymers at high rates. *Polym Eng Sci* 1978; 18: 833–839.
37. Tvergaard V and Needleman A. Effect of material rate sensitivity on failure modes in the charpy v-notch test. *J Mech Phys Solids* 1986; 34: 213–241.
38. Tvergaard V and Needleman A. An analysis of thickness effects in the izod test. *Int J Solids Struct* 2008; 45: 3951–3966.
39. Argon A and Cohen R. Toughenability of polymers. *Polymer* 2003; 44: 6013–6032.
40. Wu SX, Mai YW, Cotterell B, et al. Ductile-brittle fracture transition due to increasing crack length in a medium carbon steel. *Acta Metallurgica et Materialia* 1991; 39: 2527–2532.
41. Anderson TL. *Fracture mechanics: fundamentals and applications*. Boca Raton, FL: CRC Press/Taylor & Francis, 2017.
42. Hertzberg R. *Deformation and fracture mechanics of engineering materials*. New York: John Wiley, 1996.
43. Roberson DA, Perez ART, Shemelya CM, et al. Comparison of stress concentrator fabrication for 3d printed polymeric izod impact test specimens. *Additive Manufac* 2015; 7: 1–11.
44. Upadhyay K, Dwivedi R and Singh AK. Determination and comparison of the anisotropic strengths of fused deposition modeling p400 ABS. In *Advances in 3D printing & additive manufacturing technologies*. Singapore: Springer, 2016, pp.9–28.
45. Caminero M, Chacón J, García-Moreno I, et al. Impact damage resistance of 3d printed continuous fibre reinforced thermoplastic composites using fused deposition modelling. *Compos Part B Eng* 2018; 148: 93–103.
46. Sauer MJ. *Evaluation of the mechanical properties of 3D printed carbon fiber composites*. Master's Thesis, South Dakota State University, Brookings, South Dakota, USA, 2018.
47. Gardan J, Makke A and Recho N. A method to improve the fracture toughness using 3d printing by extrusion deposition. *Procedia Struct Integrity* 2016; 2: 144–151.
48. Benwood C, Anstey A, Andrzejewski J, et al. Improving the impact strength and heat resistance of 3d printed models: structure, property, and processing correlations during fused deposition modeling (FDM) of poly(lactic acid). *ACS Omega* 2018; 3: 4400–4411.
49. Messimer S, Rocha Pereira T, Patterson A, et al. Full-density fused deposition modeling dimensional error as a function of raster angle and build orientation: large dataset for eleven materials. *J Manufac Mater Process* 2019; 3: 6.
50. Yang HS, Kim HJ, Son J, et al. Rice-husk flour filled polypropylene composites: mechanical and morphological study. *Compos Struct* 2004; 63: 305–312.
51. Plackett D, Andersen TL, Pedersen WB, et al. Biodegradable composites based on l-poly lactide and jute fibres. *Compos Sci Technol* 2003; 63: 1287–1296.
52. Shunmugasamy VC, Anantharaman H, Pinisetty D, et al. Unnotched izod impact characterization of glass hollow particle/vinyl ester syntactic foams. *J Compos Mater* 2013; 49: 185–197.
53. Black JT and Kohser RA. *DeGarmo's materials and processes in manufacturing* (11th ed.). Hoboken: Wiley, 2011.